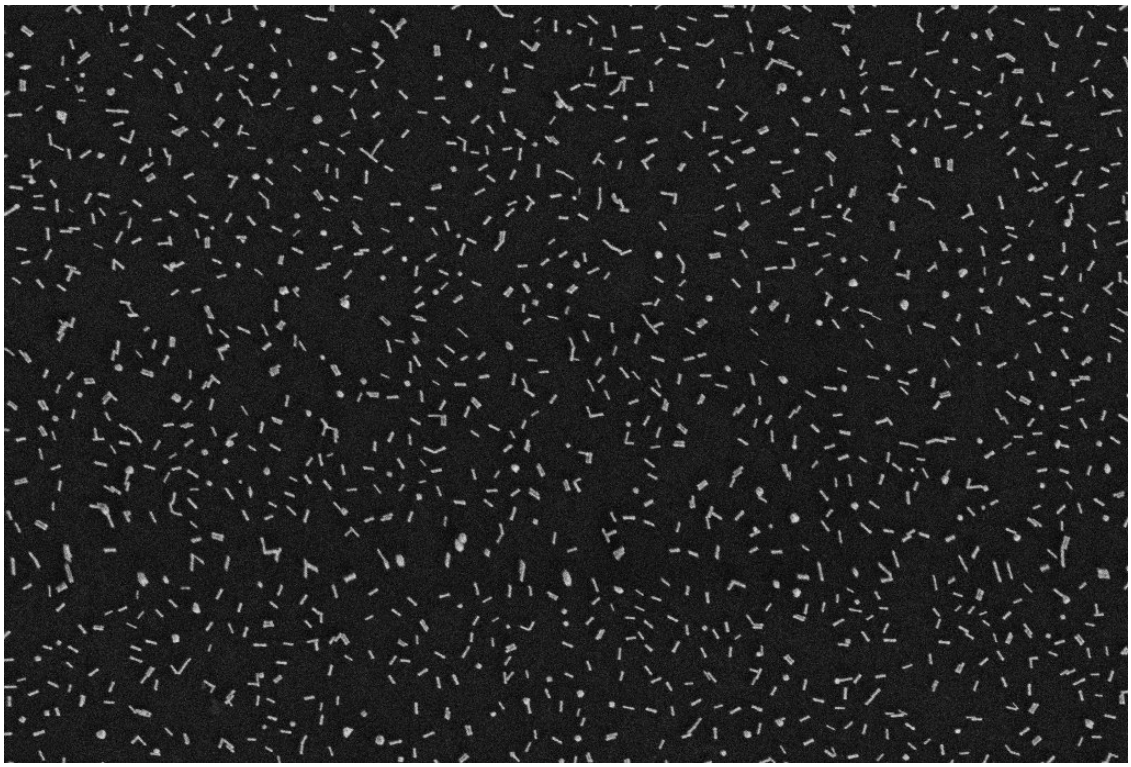

# Combining gold nanorods and antimicrobial peptides for combating biomaterial-associated infections

Master's thesis in Biomedical Engineering

JOAR WALTON

DEPARTMENT OF CHEMISTRY and CHEMICAL ENGINEERING

CHALMERS UNIVERSITY OF TECHNOLOGY
Gothenburg, Sweden 2025
www.chalmers.se

Master's thesis 2025

# Biomaterial infection elimination using gold nanorods and AMP technology

JOAR WALTON


CHALMERS
UNIVERSITY OF TECHNOLOGY

Department of Chemistry and chemical engineering
*Division of Applied chemistry*
Martin Anderssons group
Chalmers University of Technology
Gothenburg, Sweden 2025

Biomaterial infection elimination using gold nanorods and AMP technology
JOAR WALTON



Supervisor: Maja Uusitalo, Applied Chemistry
Co-supervisor: Mats Hulander, Applied Chemistry
Examiner: Martin Andersson, Applied Chemistry

Master's Thesis 2025
Department Chemistry and Chemical Engineering
Division of Applied Chemistry
Martin Andersson's group
Chalmers University of Technology
SE-412 96 Gothenburg
Telephone +46 31 772 1000

Cover: Scanning electron microscopy image of gold nanorods immobilized on a glass surface

Typeset in LaTeX
Printed by Chalmers Reproservice
Gothenburg, Sweden 2025

JOAR WALTON
Chemistry and Chemical Engineering
Applied Chemistry
Chalmers University of Technology

# Abstract

Biomaterials are materials that interact with living tissues and are widely used in modern biomedical devices such as implants. Despite their benefits, inserted biomedical implants are commonly infected by biofilm forming bacteria. Biofilms protect the bacteria from immune responses and antibiotic agents, and often require high doses of antibiotics to be eradicated. Due to patient suffering, clinical costs, and the threat of increased antimicrobial resistance, numerous developments in non-antibiotic antibacterial surface alterations has been made. This thesis investigates a biomaterial surface modification strategy utilizing surface-immobilized gold nanorods (AuNRs) and antimicrobial peptides (AMPs). AuNRs generate heat under near-infrared (NIR) irradiation, killing bacteria, while AMPs offer potent antimicrobial properties. This project aims to investigate the functionalization of AMPs onto material-supported AuNRs, and compare the combined antibacterial effect of NIR-activated AMP-AuNRs with the photothermal effect from only using AuNRs.

Material preparation included AuNR synthesis and AuNR surface immobilization. Vis-NIR spectroscopy was used to verify that the materials would exhibit a photothermal effect upon irradiation with the NIR laser, and scanning electron microscopy was used to quantify AuNR dimensions. Vis-NIR spectroscopy and water contact angle measurements showed that AMPs successfully attached to the AuNRs. The antibacterial evaluation revealed that the AMP-AuNRs did not show a synergistic bactericidal effect upon NIR laser irradiation compared to surfaces with only AuNRs. Some samples exhibited irregularities probably caused by handling errors, which limits the reliability and validity of the results. In order to draw firm conclusions, repeated testing with more rigorous experimental execution uniformity is needed. All in all, this project provided insight into AMP functionalization onto gold nanorods, as well as their antibacterial function in conjuction with photothermal agents.

Keywords: Biomaterial, biomaterial-associated infection, gold nanorod, antimicrobial peptide, visual-near infrared light, antibacterial effect

# Acknowledgements

This thesis and all of my work would not have been possible without the support of certain people. I would like to thank my supervisor Maja Uusitalo for allowing me to study her subject and contribute to her PhD. Due to your consistent feedback, open-door policy and vast knowledge I've never felt alone or lost in my project. Thanks to my co-supervisor, Mats Hulander, for your immense support in the lab, as well as always being available to discuss and help implement creative ideas or solutions. Thanks also to my examiner and group leader, Martin Andersson, for giving me the opportunity to do my thesis in your group and showing great interest whenever we had a chance to talk during the process.

Thanks to the people at the Division of Applied Chemistry for being supportive and really making me feel welcome from the very beginning. A special thanks to all the thesis workers and amanuenses I've had the pleasure to share an office with during my time at the division.

Finally, a big thanks to my family and friends for their support and encouragement. A special thank you to my girlfriend Erica, for your love and support throughout the whole thesis process.

Joar Walton, Gothenburg, January 2025

# List of Acronyms

Below is the list of acronyms that have been used throughout this thesis listed in alphabetical order:

| | |
|---|---|
| AMP(s) | Antimicrobial peptide(s) |
| AMP-AuNRs | AuNRs functionalized with AMPs |
| AuNP(s) | Gold nanoparticles |
| AuNR(s) | Gold nanorod(s) |
| BAI | Biomaterial-associated infection |
| CTAB | Hexadecyltrimethylammonium bromide |
| *E. coli* | *Escherichia coli* |
| LSPR | Localised surface plasmon resonance |
| NIR | Near infrared |
| SEM | Scanning electron microscopy |

# Contents

# List of Figures

# List of Tables

# 1
# Introduction

Biomaterials are broadly defined as materials that come in contact with living tissue, organisms, or microorganisms[1]. The use of foreign materials for therapeutic or cosmetic endeavors has been prevalent throughout most of human history. Early examples include the use of metallic dental implants in ancient Rome, and linen sutures used in ancient Egypt to stitch together large wounds[2]. Today, biomaterial science is a highly interdisciplinary field integral to modern medicine. The combination of developments in physiology, biology, chemistry, and material science has led to expansive biomaterial use for numerous medical purposes. These include implants such as joint replacements, bone defect repairs, heart valves and artificial organs; sense amplifications such as cochlear replacements and contact lenses; and surgery tools such as sutures, needles and nails.

Despite the many applications of biomaterials, there are certain risks and challenges associated with their use, one of the most prevalent being bimaterial-associated infections (BAIs) on biomedical implants. Once inserted, bacteria present at the surgical site or that has emigrated from other parts of the body can adhere to the biomaterial surface, leading to colonization and subsequent infection. Adhered bacteria can form biofilms, which are thick secretions of extracellular matrix components that act as protection from antibacterial agents such as antibiotics. Consequently, antibiotic treatments of BAIs often require high dosages which in turn leads to overuse and increased threat of antimicrobial resistance. In regards to this, numerous advancements have been made in developing non-antibiotic alterations to biomaterials which enable prevention of bacterial adhesion and infection.

In this thesis, a novel antibacterial method utilizing gold nanorods(AuNRs) and antimicrobal peptides (AMPs) was investigated. When exposed to light of their resonance wavelength, AuNRs produce heat, which can effectively kill bacteria[3]. This heat results from the oscillation of free electrons on the gold's surface, a phenomenon known as localized surface plasmon resonance (LSPR). The size and shape of the nanorod combined with the local refractive index influence the wavelength at which LSPR occurs[4]. Gold nanorods are particularly useful because their plasmon resonance falls within the biological window, in the near-infrared (NIR) range (800-2500 nm). Light in this region can pass through biological tissues and reach the nanorods inside, allowing them to generate heat and eliminate bacteria[3].

Antimicrobial peptides (AMPs) are naturally occurring molecules made up from strings of amino acids, and are found in plants, animals, and insects, known for

their potent ability to kill microorganisms[5]. In a biological environment, AMPs are rather unstable and degrade readily, limiting their effect. By binding the AMPs to AuNRs, it is hypothesised that an improved stability could be obtained. In extension, it is hypotesized that the bonds can break upon NIR irradiaton, causing release of the AMPs. In the end, the combined effect of heat and the antimicrobial properties of the AMPs could potentially lead to a more effective elimination of bacteria.

## 1.1 Aim

The aim of this thesis is to investigate AMP-functionalisation to AuNRs, as well as characterize and evaluate the combined antibacterial effect of AuNR-AMPs with near infrared light *in vitro*. In the end, we hope to see an increase in bacterial elimination efficiency from using the combined method as opposed to only using NIR-irradiated AuNRs.

# 2
# Theory

The following sections contain the relevant information needed to get acquainted with this field of research, as well as provide a background for the purposes and inner workings of the thesis. Initially, an introduction to the field of biomaterials will be presented, followed by descriptions of biomaterial-associated infections and how they could be dealt with. Following that, gold nanoparticles and their application for photothermal therapy and biomedical endeavors will be delved into, as well as a detailed description on how to synthesize gold nanorods. Finally, antimicrobial peptides will be explained, and their role in the thesis presented.

## 2.1 Biomaterials

Biomaterials are materials used for medical, therapeutic, and diagnostic purposes that come in contact with living tissue, organisms or microorganisms[1], [2]. Medical applications include implants such as artificial tissues, bones, joints, dental replacements and heart valves, as well as tissue scaffolding and *in vivo* drug delivery systems. Materials can originate from natural sources such as titanium which is often used for orthopedic implants because of its strength and rigidity. Alternatively, materials can be synthetic, such as polymers that can be chemically tuned for specific applications like drug-diffusing hydrogels or tissue scaffolds, which often require flexibility and elasticity. Biocompatibility is a characteristic common sought after when designing or applying biomaterials, and can be described as the ability to be in contact with living tissue or organisms without producing adverse effects [1], [2].

### 2.1.1 Biomaterial-associated infections

Biomaterial-associated infections (BAIs) on biomaterial surfaces are a common consequence of invasive biomaterial surgery, and are hard to treat due to the decreased antibiotic sensitivity of biofilm producing bacteria. A biofilm consists of a complicated matrix that embeds the microorganism that produces it, and contains certain proteins and molecules which protect the microorganisms from environmental stresses, antibiotics, and immune system interactions. Diagnosing such infections can be difficult, and treating them is further complicated by increased occurance of antimicrobial resistance[6]

BAIs can be classified into three categories of infections: Superficial immediate, deep

immediate, and deep late infections. Superficial immediate infections occurs on the skin during non- or minimally invasive surgeries, and are caused by bacteria present at the surgical device (e.g sutures). Deep immediate infections are a consequence of skin bacteria being relocated into the body during surgery, causing an infection shortly thereafter. Lastly, deep late infections appear months or years after surgery, and are likely a consequence of bacteria introduced at the site during surgery that become active from a dormant state, or bacteria that has relocated at the site from other parts of the body[7].

### 2.1.2 Antibacterial modifications

The rising use of biomaterials, and consequent increase of the threat of BAIs and antimicrobial resistance, has induced a growing interest in developing non-antibiotic strategies for combatting these kind of infections. Development in this field can broadly be divided into three types of antibacterial functionality: bacteria-repelling surfaces, contact-killing surfaces, and antibacterial agent-releasing surfaces[8]. Bacteria-repelling surfaces are coated with substances that prevent bacterial adhesion, often consisting of polymers such as polyethylene glycol or zwitterionic polymers. Contact-killing surface coatings consists of substances that disrupts and kill bacteria upon contact, a characteristic found in for example quaternary ammonium compounds and antimicrobial peptides(AMPs) . Lastly, antibacterial agent-releasing biomaterials are loaded with antimicrobial agents such as conventional antibiotics, AMPs or silver nanoparticles. When triggered from diffusion, dissolution or degradation of the material, the agents are released from the material and initiates their antimicrobial functions[8].

Within these categories there exists several different combinations and strategies for antibacterial effect, including therapies that utilizes coatings which exhibits antibacterial properties upon photonic absorption. One strategy utilizing this phenomenon is performed by coating a material in photothermal agents, such as noble metal nanoparticles, which generate heat when absorbing light of certain wavelengths[4].

## 2.2 Gold nanoparticles

In recent decades, gold nanoparticles (AuNPs) in have been shown to exhibit medically exploitable properties. At the nanoscale (1-100 nm), electronic motion operates differently than in bulk, which in turn affects physical and chemical behavior[4]. In the case of AuNPs, certain optical and photothermal properties arise that have been utilized for medical endeavors within fields such as sensing, imaging, and cancer therapy. The enhanced properties, high chemical and physical stability, biocompatibility, and ease of surface functionalization with organic and biological molecules, are the key characteristics behind the wide use of AuNPs in medicine today[9].

### 2.2.1 Properties

The enhanced optical and photothermal properties of AuNPs arise from oscillations of free electrons on the gold's surface in the presence of light of a certain frequency, a phenomenon known as localized surface plasmon resonance (LSPR). At the nanoscale, photons of light become confined within the particle and excites its electrons, causing the oscillation. When the oscillation decays, the energy is either radiated as scattered light or heat converted from the absorbed light. The wavelength at which LSPR occurs is dependent on electron charge density on the particle surface, which in turn is decided by particle size, shape, and dielectric properties of the material and surrounding medium[4]. Refractive index (RI) is a measurement of the light bending ability of surrounding mediums and is dependent on the speed of light in the medium. A change in RI will as such affect the LSPR frequency.

The shape of AuNPs also greatly affects the LSPR frequency and how many resonance frequencies the particle has. As depicted in figure 1[10], a gold nanosphere only exhibits one resonance direction for the LSPR to fall on, while gold nanorods (AuNRs) has two, longitudinal and transverse. Transverse LSPR produces an absorption band (transverse band) at around 500 nm, in the visible spectra. Longitudinal LSPR on the other hand produce a much stronger absorption band (longitudinal band) at the threshold between visible and near-infrared light at around 750-900 nm.

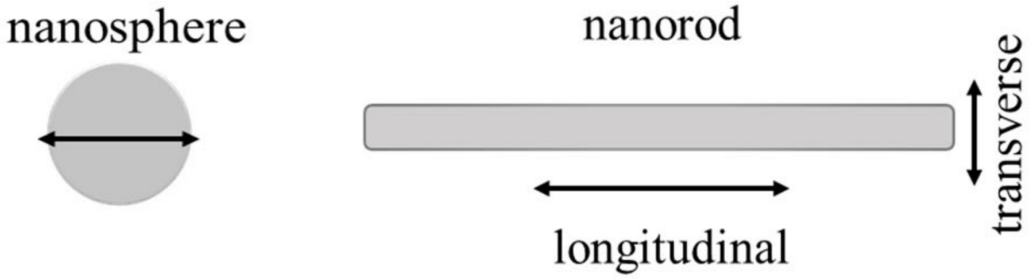


**Figure 1:** *Nanoparticles in the shape of a sphere and a rod, and their respective LSPR oscillation possibilities*[10]

#### 2.2.1.1 Phototermal applications

Phototermal applications of gold nanoparticles is based on photothermal therapy (PTT) research, where phototermal agents absorb light and converts it to heat. This heat will in turn affect the local environment surrounding the nanoparticle, and induce thermal damage to cells in its vicinity. So far, extensive research has been performed to see if this is a viable cancer treatment approach through selective localized heating of cancer cells[11], [12]. Moreover, PTT research has branched out as potential alternative to bacterial infections treatments, where bacteria in the local vicinity are killed via the heat eminating from the irradiated particle.

For noninvasive *in vivo* antibacterial application, irradiation with light of wavelengths within 600-950 nm is preferred due to major bodily contents such as water and hemoglobin expressing their lowest absorption bands in that region[13]. AuNRs express both transverse LSPR and longitiudinal LSPR frequencies, where the longitudinal gives rise to a stronger oscillation and in turn a stronger heat decay from the particles. When synthesizing AuNRs, the transverse band is largely unaffected by the size of the AuNRs, and the longitudinal band is dependent on the aspect ratio (length-to-width ratio). In general, the longitudal LSPR shifts linearly to longer wavelengths (red-shifts) as the aspect ratio increases[4].

### 2.2.2 Gold nanorod synthesis

Gold nanorods can be synthesized using a seed-mediated method using hexadecyltrimethylammonium bromide (CTAB) and silver, which is favored for its simplicity and offers fairly precise control over the aspect ratio of the nanorods. The process involves two steps: firstly, gold seeds are formed by reducing gold salt ($HAuCl_4$) with sodium borohydride in the presence of CTAB. Then, these seeds are introduced into a growth solution containing CTAB, hydrochloric acid, silver nitrate, and $Au^+$ ions, reduced from $Au^{3+}$ by ascorbic acid. Hydrochloric acid facilitates a low pH (~1.5) for the solution, which is preferable for the reduction to take place. The seeds acts as catalysts for the final reduction step from $Au^+$ to $Au^0$, allowing reduction of gold onto the already existing gold seeds and enabling formation of single-crystalline nanorods. Proposed growth mechanisms hinges on the formation of side {110} and end {100} facets when gold ions diffuses onto the seeds. It is believed that the reduction potential is lower for the {110} facet, making it the preferable facet for $Ag^+$ to be reduced on, and form a monolayer via a mechanism called underpotential deposition. This causes gold ion diffusion to only occur in the {100} direction, promoting a rod shape. CTAB also show preferential binding tendencies towards the {110} facet, further promoting a rod like shape. It also entails a positive charge for the nanorods because of its positively charged head that attach to the surface. [4], [14].

## 2.3 Antimicrobial peptides

Antimicrobial peptides (AMPs) are small molecules produced by a variety of organisms as part of their innate immune system. They are prevalent in all multicellular organisms as well as several unicellular organisms such as bacteria and viruses. [7]. Antibacterial AMPs typically consist of 10-50 amino acids and are commonly of cationic amphipatic character, meaning that their amino acids are divided into cationoic (positively charged) and non-polar regions. This property allow AMPs to target a fundamental difference between microbes and multicellular organisms, namely the cellular membrane[15].

As opposed to multicellular organisms, microbes such as bacteria exhibits a negatively charged cell membrane. A widely accepted view concerning the mechanism of

action states that electrostatic attraction causes the cationic peptides of the AMPs to bind to and penetrate the membrane. Once the membrane has been breached, the non-polar peptides then cause membrane disruption leading to lysis of the cell[16].

Given the growing issue of antibiotic resistance (AMR), AMPs are increasingly seen as a promising therapeutic alternative. Their ability to target multiple sites on the bacterial membrane, unlike conventional antibiotics who typically target specific regions on and within the bacteria, highlights their use to combat both drug-resisting bacteria, and the threat of AMR increase.

In this thesis, an antimicrobial peptide called CC-AMP (CCRRPRPRPRPWWWW, GenScript) was utilized for evaluating the synergetic effect of AuNRs and AMPs. The molecular structure of CC-AMP can be seen in figure 2. "CC" stands for the two cysteine amino acids on the end of the cationic region of the AMP. Cysteine contains a thiol group (-SH), which has shown to have a strong affinity to bind to gold surfaces, forming stable and robust connections[17].

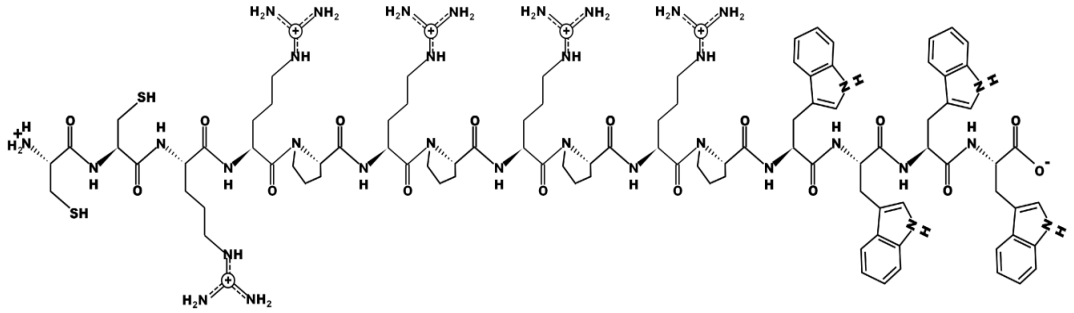

**Figure 2:** *Molecular structure of CC-AMP.*

# 3
# Methods

Initially, this chapter contains an material and chemical overview. The material preparation steps are then highlighted, namely AuNR synthesis, AuNR surface immobilization, and AMP functionalization onto the AuNRs. How these samples were utilized to test antibacterial effect is thereafter described. Finally, the different characterisation methods used throuout the experimental process are explained.

## 3.1 Materials

Chemicals used throughout the material preparation process were acquired from Sigma-Aldrich Sweden AB unless stated otherwise. The NIR-laser (BWT Beijing Ltd., model DS3-51523-50.00W) used in the antibacterial evaluation irradiated with a wavelength of 808±3 nm and was modified as described in[18]. Glassware and tweezers used in material preparation, as well as silica wafers used for preparing SEM samples were cleaned using basic piranah. Basic piranha is a mixture which, when heated, removes organic residues, metal oxides and carbonates from surfaces it contacts[19]. It consists of a 5:1:1 ratio of ultrapure water(Milli-Q, 18.2 MΩcm, Merck Millipore), ammonia($NH_3$, 28% VWR) and hydrogen peroxide 35%($H_2O_2$, Fisher Scientific). Firstly, ultrapure water and ammonia were added to the glass containers and heated to 30℃. Then, hydrogen peroxide was added and the solution was heated to 70℃, and was kept on that temperature for 15 minutes before disposal. Finally the cleaned product was thoroughly rinsed with ultrapure water and dried using nitrogen gas.

## 3.2 Gold nanorod synthesis

The synthesis was conducted according to the seed-mediated process described in 2.2.2. The seed suspension was prepared in a 30 ℃ water bath by adding 25 µL of 50mM gold(III) chloride ($HAuCl_4$) in 4.7 ml of 100 mM hexadecyltrimethylammonium bromide (CTAB). After mixing until homogeneity was achieved, 300 µL of 10mM sodium borohydride was added under strong stirring (RPM>1200), reducing the $Au^{3+}$ ions into small (d<5 nm) single-crystalline gold nuclei. The seed suspension was then kept at 30 ℃ until it was added to the growth solution.
To prepare the growth solution, 1.14 ml of 1 M hydrochloric acid and 600 µL of 50 mM $HAuCl_4$ were added to 60 ml of 100mM CTAB solution, and were thereafter mixed until homogeneity. Afterwards, 720 µL of 7 mM silver nitrate and 600 µL of 116 mM ascorbc acid were added and reduction from $Au^{3+}$ ions to $Au^{+}$ occurred,

finalizing the growth solution. Lastly. 144 µL of the seed suspension was thoroughly mixed into the growth solution, catalyzing the final reduction step from $Au^+$ to $Au^0$. The final product was then left undisturbed in a 30 ℃ water bath for 2 hours during which the nanorod formation occurred. [14].

### 3.2.1 Purification

To separate the desired nanorods from reaction mixture such as CTAB or misformed nanostructures, a purification scheme consisting of three separate centrifugations was conducted. Initially the solution was centrifuged at 1900 xg for 30 minutes at 28 ℃, after which the pellet containing the gold nanorods were collected and redispersed in ultrapure water. Centrifuging and dispersion was repeated two more times at 1800 xg for 35 minutes, resulting in a solution of gold nanorods with longitudinal resonance bands at around 850 nm (NIR region), as well as a large ratio between absorbance values at the different LSPR band, ensuring a low amount of byproducts and high purification[14].

## 3.3 Surface immobilization

The substrates (glass cover slips, 13 mm diameter, VWR) were rinsed with 95% ethanol(Solveco AB) followed by ultrapure water and were then dried using nitrogen gas ($N_2$). They were then placed in a glass petri dish containing nitric acid (65-67%) and left overnight (~18h). After the nitric acid immersion, the substrates were thoroughly rinsed with ultrapure water before being immersed in AuNR suspension. After 5 hours, a gradual exchange from AuNR solution to ultrapure water was performed, followed by immersion in 99.5% ethanol and air drying.

## 3.4 Antibacterial activity evaluation

In the final experimental phase, a comparison between the antibacterial effect of glass supported AuNRs with and without AMPs upon irradiation with NIR light was conducted *in vitro*. Sterilization and CTAB removal was conducted for all the samples by UV/$O_3$-treatment for 5 minutes prior to the experiment, which is a method to remove organic residue using ultraviolet light and ozone. Afterwards, some samples were functionalized with AMPs by immersion in 0.2 mg/ml CC-AMP solution for 2 hours, followed by rinsing with ultrapure water, then EtOH, and lastly drying with $N_2$ gas. For bacterial cultivation, an agar plate model using *Escherichia coli* (*E. coli*)CCUG 29300T, was used[20]. In short, frozen *E. coli* was streaked onto a brain heart infusion (BHI) agar plate and incubated at 37℃ overnight. One colony was thereafter inoculated in tryptic soy broth and put in incubation at 37 ℃. When the bacterial inoculum reached an OD of 0.50-0.55 (measured using a optical density reader), it was subsequently diluted in phosphate buffer to a concentration of approximately $5x10^4$ colony forming units (CFU)/ml. The final bacterial suspension was thereafter streaked onto BHI agar plates using cotton swabs. Samples were then placed onto the agar plates with the functionalized side facing down on the bacteria,

and some were subsequently irradiated with a NIR laser at 808 nm for 30 seconds. Different laser intensities were used for different samples, and a schematic illustrating the experimental setup is shown in figure 3. After irradiation, the bacterial plates were placed in incubation overnight at 37 ℃. Finally, the day after, pictures were taken of the plates, and CFUs under each plate were counted. To ensure comparable and replicable data, all samples were done in triplicates on three separate occasions, and for each experiment the order of NIR irradiation was randomized to avoid biased data.

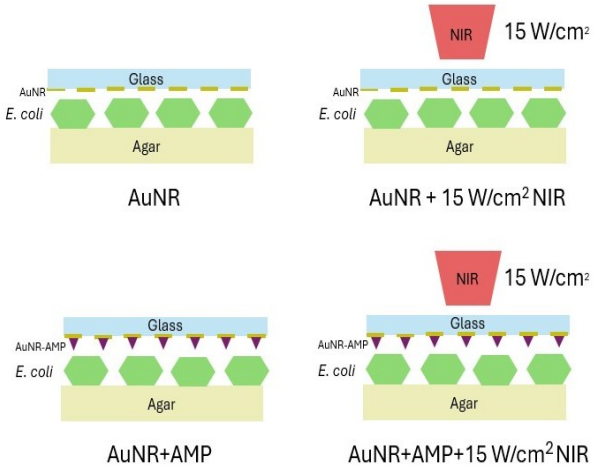


**Figure 3:** *Experimental setup for the bacterial elimination study*

## 3.5 Characterisation

### 3.5.1 Vis-NIR spectroscopy

Vis-NIR spectroscopy is performed by beaming light of wavelengths within the visible and near-infrared spectra (350-2500nm) through a sample, and measuring the amount of light that passes through. Absorbance is a measure of how much light is absorbed by the sample, and is dependent on its properties and concentration. For the purpose of this thesis, Vis-NIR spectroscopy was used to locate the longitudinal LSPR band of AuNRs (in suspension), ensuring it fell in the range of the NIR laser (825-850 nm). Furthermore, Vis-NIR was also used to analyze AuNR surface immobilization and AMP functionalization. Absorption spectra for AuNR suspensions were measured on a Mutiskan GO Microplate Spectrophotometer (Thermo Fisher). Absorption spectra for AuNRs immbobilized on glass and AMP functionalization onto the AuNRs were measured in air using a Cary 60 UV-vis spectrometer(Agilent Technologies). All measurments performed were done in ranges of 400-1000 nm.

### 3.5.2 Scanning electron microscopy

A Scanning Electron Microscope (SEM) utilizes a highly energized electron beam to scan sample surfaces in a vacuum. Interactions between the sample and the electron beam generate signals such as secondary, backscattered, or Auger electrons, x-rays and sometimes light. These signals are then detected by their respective detector. Secondary electrons come from the sample surface and primarily give topological and spatial information. Backscattered electrons emerge from deeper into the sample, and provide compositional information. Auger electrons and x-rays are emitted from atomic layers very close to the surface, and give information regarding surface chemistry and chemical composition, respectively[21]. In this thesis, a Zeiss Ultra Scanning electron microscope was used, along with the ImageJ analysis program, to determine parameters such as AuNR lengths, widths, aspect ratios, and surface coverages. As spatial dimensions were of most interest, secondary electron detection was employed to image the samples.

### 3.5.3 Contact angle

Contact angle measurements were carried out in addition to Vis-NIR spectroscopy to verify AMP functionalization onto the AuNRs. It is a simple but effective method to measure the hydrophilicity of a surface, and is conducted by putting a drop of water onto a surface, and measuring of the angle between the droplet and the surface, a principle illustrated in figure 4. On a hydrophilic surface, the drop tends to spread out and produce a small angle, whereas a drop on a hydrophobic surface is repelled and does not spread, resulting in higher contact angles[22].

To verify AMP functionalization, AuNR-immobilized glass surfaces were initially UV/$O_3$-treated for 5 min. Afterwards, some AuNR-surfaces were immersed in AMP solution, and some were immersed in ultrapure water. A contact angle comparison using an Attension optical goniometer was then conducted in order to see the potential changes that the AMP treatment had on the hydrophilicity of the surfaces.

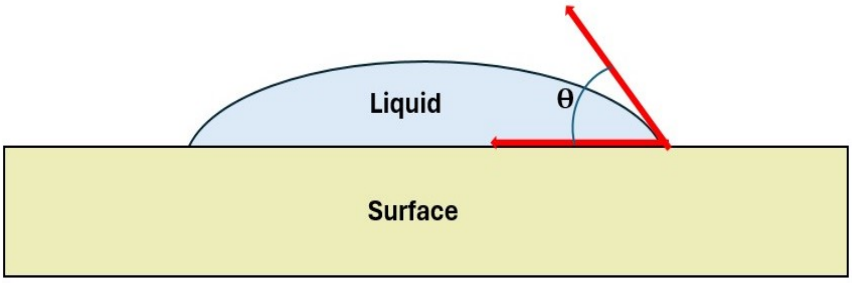


**Figure 4:** *Illustration covering the highlighted parts of performing a contact angle measurement.*

# 4

# Results and discussion

Experimentally, this thesis was divided into four different parts: AuNR synthesis, AuNR surface immobilization, AMP functionalization onto the AuNRs, and antibacterial effect comparisons between non-AMP-functionlized AuNRs and AMP-functionlized AuNRs.

## 4.1 AuNR synthesis

The AuNR synthesis resulted in suspensions of AuNR with a longitudinal LSPR band at 838 nm, and a high ratio (~1:4) between the two LSPR bands, indicating of high purification and few byproducts (fig.5A). The ratio of AuNRs and unwanted byproducts (i.e. nanospheres) was also analyzed using SEM, shown in figure 5B, where most of the nanoparticles present are of rod-like shape.

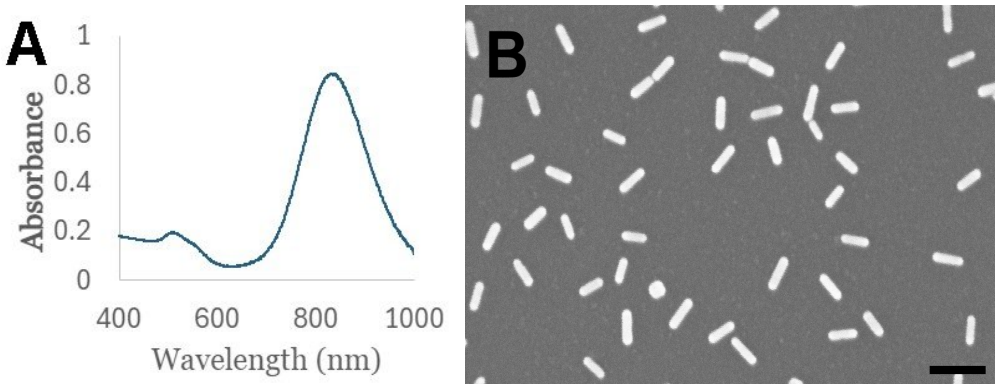


**Figure 5:** *(A) Vis-NIR absorption spectra of gold nanorods in aqueous solution, and (B) SEM image of gold nanorods on a silica wafer. Scale bar is 100 nm.*

Using SEM images, and the particle analysis tool ImageJ, measurements of AuNR lengths, widths and aspect ratios (length/width) were performed, and are summarized in Table 1. According to previous research, an aspect ratio of around 4 is typically what entails a longitudinal LSPR expression at the NIR laser wavelength used (808nm)[4], [18]. The result from this synthesis therefore somewhat contradicts these studies, although the low resolution in SEM images is a major error source. For a proper dimensional analysis, utilizing Transmission electron microscopy would be preferred.

| | Length (nm) | Width (nm) | Aspect Ratio |
|---|---|---|---|
| **AuNRs** | 53.4 ± 4.7 | 20.2 ± 2.0 | 2.7 ± 0.3 |

**Table 1:** AuNR measurments from 100 different rods, depicted as the mean±standard deviation.

## 4.2 AuNR glass immobilization

To verify immobilization of the AuNRs onto glass, NIR-Vis spectroscopy in air and SEM imaging were used (Fig.6). The absorption spectrum (Fig.6A) indicated that AuNRs had bound to the surface and had retained their plasmonic properties. Compared to figure 5A, the spectra exhibits certain differences, mainly a low absorption value, and a blue-shifted longitudinal LSPR band (maximum at 759 nm). The low absorption value is caused by switching from measuring a concentrated suspension where AuNRs are in abundance, to measuring the low concentration monolayer formed on the glass surface. The difference in refractive index (see 2.2.1), from an aqueous solution in figure 5A to an air-glass interface in figure6A, is what caused the blue-shift to occur.

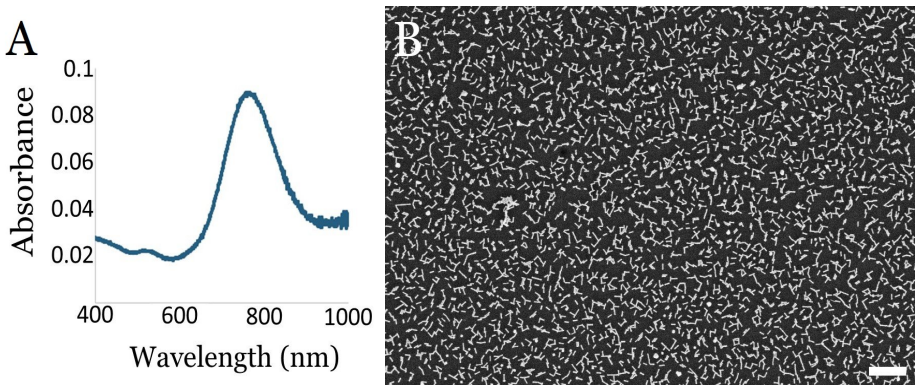


**Figure 6:** *Characterisation of AuNR immobilization. (A) Vis-NIR absorption spectrum of AuNRs supported on glass in air, and (B) SEM image of AuNR distribution and coverage of the surface. Scale bar is 400 nm*

SEM photography revealed the distribution of immobilized AuNRs across the glass surfaces. In figure6, an example is shown that expressed a surface coverage of 19%. The AuNRs lie fairly tightly, and appear to be forming many small aggregates. Aggregates give rise to a phenomenon known as plasmon coupling, where resonance bands of close-lying particles interact and potentially shift. For samples such as the one depicted in figure 6B, plasmon coupling could potentially affect the antibacterial efficacy when irradiated with the 808 nm laser.

## 4.3 AMP functionalization

AMP functionalization onto AuNRs immobilized on glass surfaces was performed using the method described in section 3. By firstly treating the AuNR coated surfaces in an UV/$O_3$ oven, the CTAB covering the AuNRs was removed, leaving behind a pure gold surface with which the CC-AMPs could readily form thiol bonds. To verify this interaction, two methods were used: contact angle measurement and Vis-NIR spectroscopy in air. Contact angle measurements were conducted with the intention of visualizing how AMP functionalization affects the hydrophilicity of the surfaces. Figures 7A-B are taken of milli-Q water droplets on surfaces that had been submerged in ultrapure water (A), as well as 0.2 mg/ml CC-AMP solution (B). Table 2 summarizes the contact angle measurements for all samples that were tested. The results indicate that the surfaces became more hydrophobic after AMP treatment, as the average contact angle increased. Assuming AMP functionalization onto the AuNRs took place, this is also what was expected. As described in section 2.3, AMPs contain both hydrophobic and hydrophilic regions. For CC-AMP in particular, its the hydrophilic part of the chain that contains the cysteine amino acids which forms thiol bonds with the AuNRs, leaving the hydrophobic region to interact outwards from the particles. While the number of samples tested were low (n=2), the results show that AMP functionalization onto the AuNRs probably occurred, and that using surfaces treated with CC-AMP in this manner for antibacterial purposes is a valid continuation of the process.

| | Plain glass | UV/$O_3$ | Milli-Q ($\mu$, n=2) | AMP ($\mu$, n=2) |
|---|---|---|---|---|
| **Contact Angle (°)** | 23.4 | 13.2 | 15.2 | 31.3 |

**Table 2:** Mean contact angle for glass surfaces in different experimental phases.

By functionalizing AMPs onto the AuNRs, a red-shift of the resonance peak was expected to occur due to increase in local refractive index from surrounding the AuNRs with AMPs[23]. In the Vis-NIR spectrum illustrated in figure 7C, a 20 nm red-shift of the longitudinal LSPR band appeared. Another notable difference is that the maximal absorbance value slightly decreased. This could potentially be due to small disruptions of the AuNR monolayer during the AMP functionalization process, such as rods detaching or aggregates forming, both of which would cause absorption decreases.

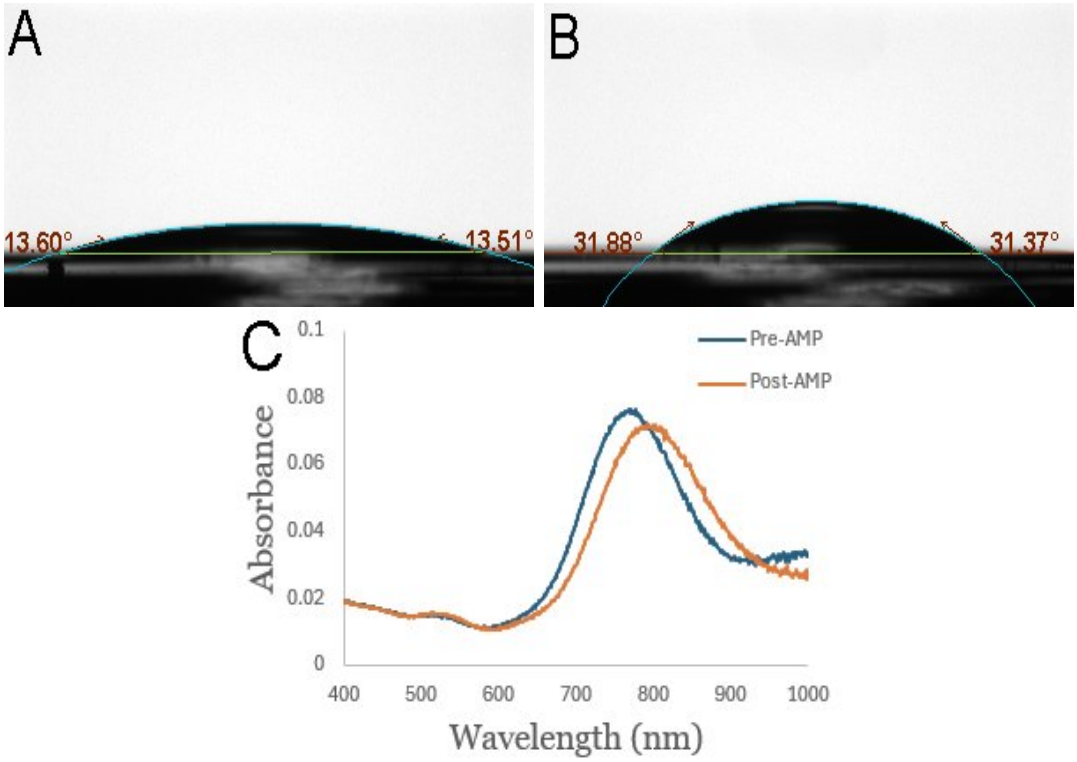


**Figure 7:** *Contact angles for ultrapure water droplet on (A) on a surface pre-AMP and (B) post-AMP treatment. (C) Mean absorption spectra in air (n=3) of surfaces pre-AMP (blue) and post-AMP (orange) treatment.*

## 4.4 Antibacterial evaluation

The antibacterial effect of each group was determined by counting the number of colony forming units (CFUs) under the samples, calculating the parameter CFU/cm$^2$, and then analyzing the results using a two-sample t-test assuming equal variances. The four groups tested were: AuNRs 0W/cm$^2$, AMP-AuNRs 0W/cm$^2$, AuNRs 15W/cm$^2$, and AMP-AuNRs 15W/cm$^2$. In one of the triplicate runs of the experiment, the NIR laser lid was not taken of before irradiaton, causing samples that would have been irradiated to become obsolete. Therefore, the amount of samples for the irradiated groups are 6 each, as opposed to 9 in the non-irradiated groups. A summary of the results of the antibacterial evaluation is illustrated in figure 8. It showed that using the NIR laser at 808 nm and 15 W/cm$^2$ for 30 seconds caused AuNRs to express plasmonic properties and photothermal eradication of bacteria, compared to non-irradiated groups. On average, irradiated AuNRs displayed a 59% and 49% reduction in CFU/cm$^2$ against non-irradiated AuNRs and AMP-AuNRs, respectively. Irradiated AMP-AuNRs displayed a 55% reduction compared to non-irradiated AuNRs on average.

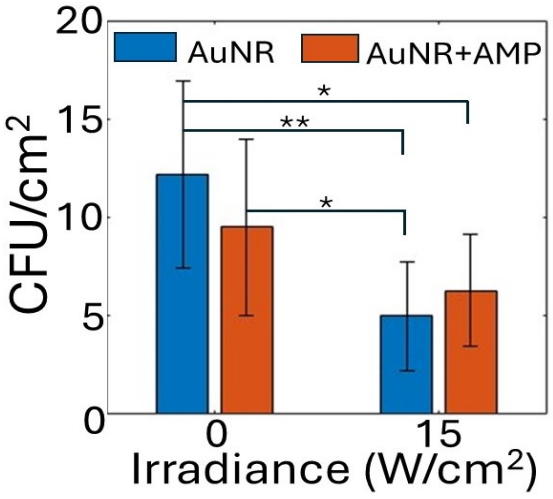


**Figure 8:** *Summary of the antibacterial evaluation visualizing the statistical differences between the tested groups, in terms of CFU/cm$^2$. Bars depict the mean (n=9 for non-irradiated, and n=6 for irradiated), and error bars show standard deviation. Significance level (**)p<0.01, (*)p<0.05*

While the statistical analysis shows results in line with what was hypothesised, except that AMP-AuNRs did not show an enhanced synergetic effect, it does not tell the whole story. Small sample groups, human error and potential irregularities throughout the process, are all error sources that need to be discussed. Figure 9 show outtakes from each sample group (all sample photos can be found in appendix A), and from these photos we can notice a few irregularities and non-expected results. Starting with the irregularities, samples such as figure 9B,D,F,H,O,P seem to have been obstructed in some way, causing large bubbles to appear underneath the samples. Since no bacterial colonies can be seen where the bubbles are located, this obstruction likely impedes bacterial growth. While the cause is unknown, a theory could be that the tweezers used to place the samples onto the plate were not rid of all of the ethanol (from being sterilized) prior to sample management, causing some ethanol drops to get trapped under the samples. This would explain the antibacterial property and shapes of the bubbles. Another obstruction was observed in figures 9F,O, where a minor gash is apparent on under each sample. It looks to be physical damage, probably coming from either reckless handling of the tweezers or sample upon laying it on the bacterial plate. These gashes does not appear to impede colony formation however.

In terms of inconsistent or unexpected results, a couple of samples stand out. Samples 9G-H were not irradiated with with the laser, but nonetheless seem to express antibacterial activity over large parts of their surface area. Since non-irradiated AuNRs does not show any antibacterial effect, this could suggest that AMPs have a slight tendency to exhibit their antibacterial properties despite not being released from the AuNRs. However, this theory is highly speculative, and needs further testing for verification. Looking at the irradiated AuNR samples in figures 9K-L, bacterial growth is apparent even though it was not expected. This is likely due to uneven surface coverage of the AuNRs or the prevalence of large AuNR aggre-

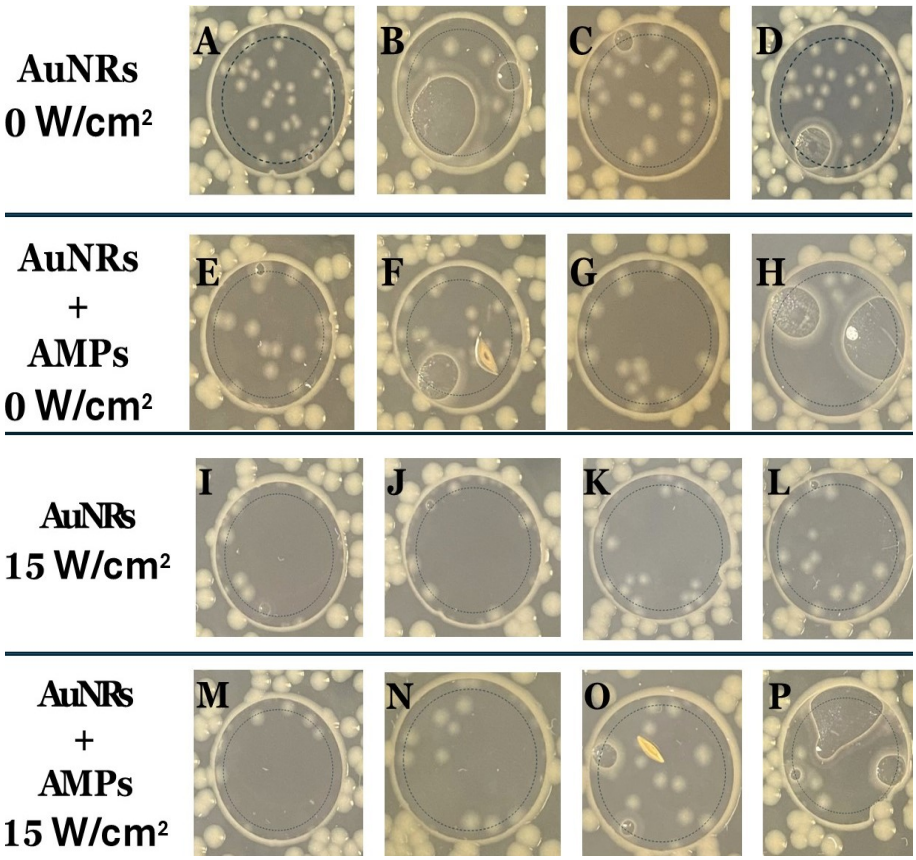


**Figure 9:** *Outtakes from the antibacterial evaluation, showing four samples from each of the tested groups. (A-D) non-iradiated AuNRs (E-H) non-irradiated AMP-AuNRs (I-L) 30s 15 W/cm$^2$ irradiated AuNRs (M-P)30s 15 W/cm$^2$ irradiated AMP-AuNRs. Sampling area is depicted by a dashed black circle.*

gate formations. As explained in section 4.2, tightly packed AuNRs might influence each other's optical properties via plasmon coupling, potentially shifting the longitudinal LSPR to frequencies away from the 808 nm laser. Similarly, AMP-AuNR samples in figures 9N-O also show abundant bacterial growth. In addition to the factors described above, this could also be caused by AMPs somehow impeding the antibacterial effect of irradiated AuNRs, or that the AuNRs were obstructed or removed during AMP functionalization. Similar to the contact angle study, further testing of this interaction could be performed by analyzing the antibacterial effect of AuNR samples that have undergone AMP functionalization treatment, however using ultrapure water instead of AMP-solution.

## 4.5 Future aspects

The combination of small sample groups and inexperience in experimental execution greatly limits the reliability of the antibacterial evaluation. Further testing using the same setups and protocols would undoubtedly need to be performed in order to draw firm conclusions. For this thesis, the antibacterial properties of CC-AMPs in conjunction with AuNRs were of most interest. Additional experiments would give further and more reliable insight regarding potential antibacterial properties of CC-AMPs on both non-irradiated and irradiated samples.

It is difficult to pinpoint the reason AMP displayed a negligible difference in the results of the antibacterial evaluation study performed in this thesis. Apart from human errors, it could perhaps be that CC-AMP do not express any antibacterial activity towards *E. coli*, or that the concentration of AMPs on the AuNR surfaces was too low. To test for antibacterial activity, a minimum inhibitory concentration protocol could be employed. It would provide valuable knowledge of both antbacterial effect and its concentration dependency.

Once firm and reliable conclusions concerning interactions between CC-AMP and *E. coli* in the context of these experiments has been made, branching outwards by using other biofilm forming bacteria is the next logical step. An interesting aspect would be if there is a difference in antibacterial effect between gram-negative and gram-positive bacteria. Tests regarding cytotoxicity and other, more biomedically viable materials would also be imperative to understand how the method fares in bioloical environments.

# 5
# Conclusion

The aim of this thesis was to investigate AMP-functionalisation to AuNRs, as well as characterize and evaluate the combined antibacterial effect of AuNR-AMPs with near infrared light *in vitro*.. By using Vis-NIR spectroscopy and contact angle measurements, AMP functionalisation onto AuNRs could be detected. A longitudinal LSPR red-shift was clearly noted in the Vis-NIR spectrum, and water contact angle essentially doubled when compared with non-functionalized glass-supported AuNRs.

The antibacterial evaluation showed that both AuNRs and AMP-AuNRs irradiated at 808 nm and 15 W/cm$^2$ possess a significant antibacterial effect compared to non-irradiated AuNRs. AMP-AuNRs did not show any significant antibacterial effect compared to AuNRs in their respective irradiation group (0 and 15 W/cm$^2$). Whether this is due to experimental mishaps and human errors, or impeded antibacterial activity from the test conditions, is unclear, and needs to be further investigated upon. Nevertheless, this thesis provided relevant knowledge surrounding the integration of AMPs with NIR irradiated AuNRs, laying certain groundwork for the method going forward.

# Bibliography


[1] M. Vert, Y. Doi, K.-H. Hellwich, *et al.*, "Terminology for biorelated polymers and applications (IUPAC Recommendations 2012)," *Pure and Applied Chemistry*, vol. 84, no. 2, pp. 377–410, Jan. 2012, ISSN: 1365-3075. DOI: 10.1351/PAC-REC-10-12-04.

[2] B. D. Ratner and G. Zhang, "A History of Biomaterials," in *Biomaterials Science*, Elsevier, 2020, pp. 21–34. DOI: 10.1016/B978-0-12-816137-1.00002-7.

[3] T. Yang, D. Wang, and X. Liu, "Assembled gold nanorods for the photothermal killing of bacteria," *Colloids and Surfaces B: Biointerfaces*, vol. 173, pp. 833–841, Jan. 2019, ISSN: 09277765. DOI: 10.1016/j.colsurfb.2018.10.060. [Online]. Available: https://www.sciencedirect.com/science/article/pii/S0927776518307586.

[4] X. Huang, S. Neretina, and M. A. El-Sayed, "Gold Nanorods: From Synthesis and Properties to Biological and Biomedical Applications," *Advanced Materials*, vol. 21, no. 48, pp. 4880–4910, Dec. 2009, ISSN: 0935-9648. DOI: 10.1002/adma.200802789.

[5] M. Zasloff, "Antimicrobial peptides of multicellular organisms," *Nature*, vol. 415, no. 6870, pp. 389–395, Jan. 2002, ISSN: 0028-0836. DOI: 10.1038/415389a.

[6] C. R. Arciola, D. Campoccia, and L. Montanaro, "Implant infections: adhesion, biofilm formation and immune evasion," *Nature Reviews Microbiology*, vol. 16, no. 7, pp. 397–409, Jul. 2018, ISSN: 1740-1526. DOI: 10.1038/s41579-018-0019-y.

[7] F. Costa, I. F. Carvalho, R. C. Montelaro, P. Gomes, and M. C. L. Martins, "Covalent immobilization of antimicrobial peptides (AMPs) onto biomaterial surfaces," *Acta Biomaterialia*, vol. 7, no. 4, pp. 1431–1440, Apr. 2011, ISSN: 17427061. DOI: 10.1016/j.actbio.2010.11.005.

[8] C. Zhao, L. Zhou, M. Chiao, and W. Yang, "Antibacterial hydrogel coating: Strategies in surface chemistry," *Advances in Colloid and Interface Science*, vol. 285, p. 102 280, Nov. 2020, ISSN: 00018686. DOI: 10.1016/j.cis.2020.102280.

[9] M. B. Almeida, C. M. R. Galdiano, F. S. R. d. Silva Benvenuto, E. Carrilho, and L. C. Brazaca, "Strategies Employed to Design Biocompatible Metal Nanoparticles for Medical Science and Biotechnology Applications," *ACS Applied Materials & Interfaces*, vol. 16, no. 49, pp. 67 054–67 072, Dec. 2024, ISSN: 1944-8244. DOI: 10.1021/acsami.4c00838. [Online]. Available: https://pubs.acs.org/doi/10.1021/acsami.4c00838.

[10] P. Khan, G. Brennan, J. Lillis, S. A. M. Tofail, N. Liu, and C. Silien, "Characterisation and Manipulation of Polarisation Response in Plasmonic and Magneto-Plasmonic Nanostructures and Metamaterials," *Symmetry*, vol. 12, no. 8, p. 1365, Aug. 2020, ISSN: 2073-8994. DOI: 10.3390/sym12081365.

[11] X. Huang, P. K. Jain, I. H. El-Sayed, and M. A. El-Sayed, "Plasmonic photothermal therapy (PPTT) using gold nanoparticles," *Lasers in Medical Science*, vol. 23, no. 3, pp. 217–228, Jul. 2008, ISSN: 0268-8921. DOI: 10.1007/s10103-007-0470-x.

[12] P. K. Jain, X. Huang, I. H. El-Sayed, and M. A. El-Sayed, "Noble Metals on the Nanoscale: Optical and Photothermal Properties and Some Applications in Imaging, Sensing, Biology, and Medicine," *Accounts of Chemical Research*, vol. 41, no. 12, pp. 1578–1586, Dec. 2008, ISSN: 0001-4842. DOI: 10.1021/ar7002804.

[13] R. Weissleder, "A clearer vision for in vivo imaging," *Nature Biotechnology*, vol. 19, no. 4, pp. 316–317, Apr. 2001, ISSN: 1087-0156. DOI: 10.1038/86684.

[14] L. Scarabelli, A. Sánchez-Iglesias, J. Pérez-Juste, and L. M. Liz-Marzán, "A "Tips and Tricks" Practical Guide to the Synthesis of Gold Nanorods," *The Journal of Physical Chemistry Letters*, vol. 6, no. 21, pp. 4270–4279, Nov. 2015, ISSN: 1948-7185. DOI: 10.1021/acs.jpclett.5b02123. [Online]. Available: https://pubs.acs.org/doi/10.1021/acs.jpclett.5b02123.

[15] A. Bahar and D. Ren, "Antimicrobial Peptides," *Pharmaceuticals*, vol. 6, no. 12, pp. 1543–1575, Nov. 2013, ISSN: 1424-8247. DOI: 10.3390/ph6121543.

[16] J. Xuan, W. Feng, J. Wang, *et al.*, "Antimicrobial peptides for combating drug-resistant bacterial infections," *Drug Resistance Updates*, vol. 68, p. 100 954, May 2023, ISSN: 13687646. DOI: 10.1016/j.drup.2023.100954.

[17] M. Borzenkov, G. Chirico, L. D'Alfonso, *et al.*, "Thermal and Chemical Stability of Thiol Bonding on Gold Nanostars," *Langmuir*, vol. 31, no. 29, pp. 8081–8091, Jul. 2015, ISSN: 0743-7463. DOI: 10.1021/acs.langmuir.5b01473.

[18] M. Uusitalo, M. Strach, G. Eriksson, *et al.*, "Photothermal Properties of Solid-Supported Gold Nanorods," *Nano Letters*, vol. 24, no. 40, pp. 12 529–12 535, Oct. 2024, ISSN: 1530-6984. DOI: 10.1021/acs.nanolett.4c03472.

[19] H. G. Schmidt, "Safe Piranhas: A Review of Methods and Protocols," *ACS Chemical Health & Safety*, vol. 29, no. 1, pp. 54–61, Jan. 2022, ISSN: 1871-5532. DOI: 10.1021/acs.chas.1c00094.

[20] G. A. Buckholtz, N. A. Reger, W. D. Anderton, *et al.*, "Reducing Escherichia coli growth on a composite biomaterial by a surface immobilized antimicrobial peptide," *Materials Science and Engineering: C*, vol. 65, pp. 126–134, Aug. 2016, ISSN: 09284931. DOI: 10.1016/j.msec.2016.04.021.

[21] K. Vernon-Parry, "Scanning electron microscopy: an introduction," *III-Vs Review*, vol. 13, no. 4, pp. 40–44, Jul. 2000, ISSN: 09611290. DOI: 10.1016/S0961-1290(00)80006-X. [Online]. Available: https://www.sciencedirect.com/science/article/pii/S096112900080006X.

[22] S. A. D. M. Zahir, A. F. Omar, M. F. Jamlos, M. A. M. Azmi, and J. Muncan, "A review of visible and near-infrared (Vis-NIR) spectroscopy application in plant stress detection," *Sensors and Actuators A: Physical*, vol. 338, p. 113 468, May 2022, ISSN: 09244247. DOI: 10.1016/j.sna.2022.113468.

[23] H. Zhang, P. Cao, J. Dou, L. Cheng, T. Niu, and G. Zhang, "Double-exponential refractive index sensitivity of metal-semiconductor core-shell nanoparticles: the effects of dual-plasmon resonances and red-shift.," *RSC advances*, vol. 8, no. 3, pp. 1700–1705, Jan. 2018, ISSN: 2046-2069. DOI: 10.1039/c7ra11981j.

# A

# Appendix 1

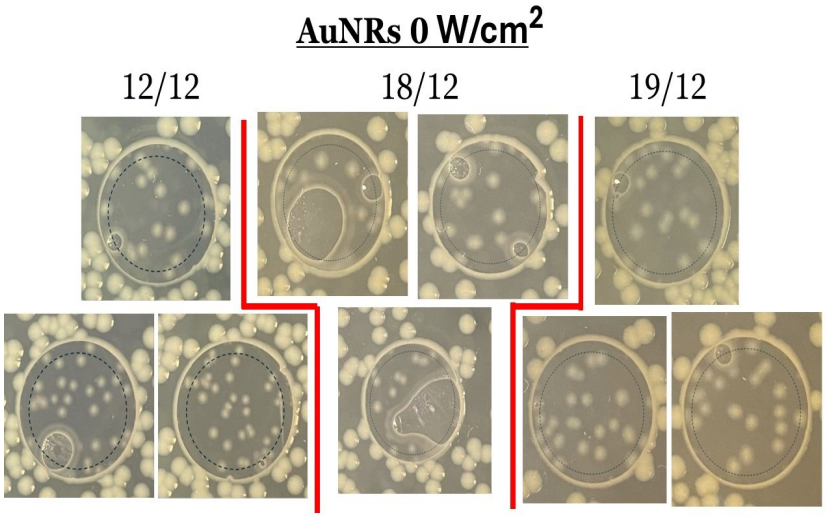


**Figure 10:** *All samples of AuNRs 0 W/cm$^2$.*

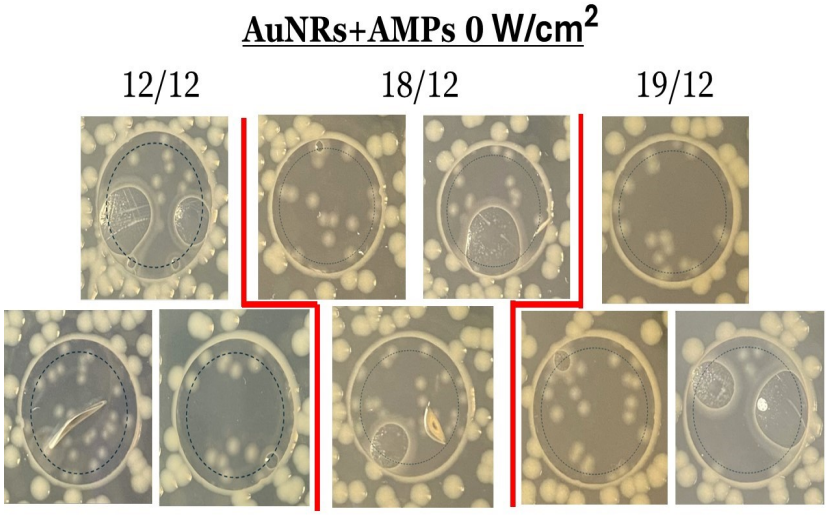


**Figure 11:** *All samples of AMP-AuNRs 0 W/cm$^2$.*

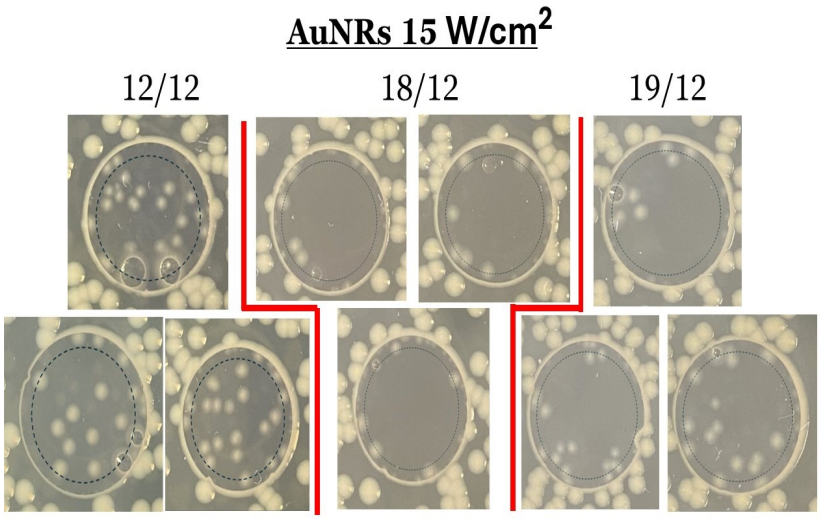


**Figure 12:** *All samples of AuNRs 15 W/cm$^2$. Note that samples under 12-12 were not irradiated to to the laser beam being obstructed.*

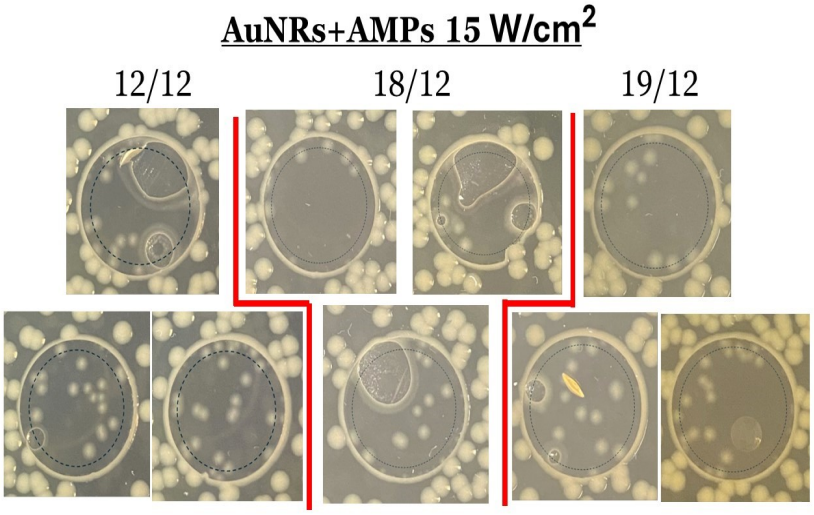


**Figure 13:** *All samples of AMP-AuNRs 15 W/cm$^2$. Note that samples under 12-12 were not irradiated to to the laser beam being obstructed.*

**DEPARTMENT OF Chemistry and Chemical Engineering**
**CHALMERS UNIVERSITY OF TECHNOLOGY**
Gothenburg, Sweden
www.chalmers.se


CHALMERS
UNIVERSITY OF TECHNOLOGY